Quantized excitation spectra by magnon confinement in quasi-one-dimensional $S = 1$ spin systems

Takafumi Suzuki and Sei-ichiro Suga

Graduate School of Engineering, University of Hyogo, Himeji 671-2280, Japan

The infinite time-evolving block decimation algorithm is applied to calculate the dynamical spin-structure factors of the quasi-one-dimensional (Q1D) $S = 1$ antiferromagnetic spin system with single-ion anisotropy and bond alternation. It is found that when the staggered field induced by the weak interchain interaction is taken into account, the excitation continuum originating from magnons is quantized. The excitation energies of the quantized excitation spectra are well explained by the negative zeros of the Airy functions, when the single-ion anisotropy is negatively strong. This quantization of the magnon continuum is a counterpart of the spinon confinement, which has been recently discussed for Q1D $S = 1/2$ antiferromagnets. It is further shown that, when a staggered field exists, the quantized excitation spectra appear on the phase boundary between the Haldane and Néel phases of the phase diagram without the staggered field. However, the quantized excitation spectra disappear in the singlet-dimer phase.

Recent inelastic neutron scattering (INS) experiments [1,2] on quasi-one-dimensional (Q1D) $S = 1/2$ antiferromagnetic (AF) Ising-like XXZ magnets, $(Ba/Sr)Co_2V_2O_8$ [3], have reported that, below the Néel temperature T_N, these materials show quantized excitation spectra with excitation energies that are well explained by the series of negative zeros in the Airy function (NZAF). McCoy and Wu argued the relation between the NZAF and confinement of the domain-wall excitations by focusing on the excitation spectra of the $S = 1/2$ ferromagnetic (FM) Ising chain in weak transverse and longitudinal magnetic fields [4,5]. Since the ground state of this model is a fully polarized state, low-energy excitation is achieved by flipping spins of arbitrary lengths, i.e., two domain-wall excitations. Since each domain wall carries $\Delta S = 1/2$, the low-energy excitation is interpreted as two-spinon excitation. In the transverse field, these two spinons travel in the chain and compose an excitation continuum. When the uniform longitudinal field is further applied weakly, it works as a linear potential between the two spinons. The effective model for this two-spinon excitation is exactly solvable and the eigenvalues are given by NZAF [4,5]. This means that the excitation spectra of the two-spinon continuum are quantized. The quantized spectra explained by NZAF have been confirmed in the INS experiments [6] on $CoNb_2O_6$, which is a ferromagnetic Ising spin-chain compound. Shiba also discussed the quantized excitation spectra in the Q1D $S = 1/2$ AF Ising-like XXZ system [7]. When we focus on bipartite systems, the interchain interaction in the Q1D AF systems effectively works as a weak staggered field below T_N. Thus, it is expected that the domain-wall excitations along the spin-chain direction are confined by the weak staggered field and that the same discussion as that for the ferromagnetic Ising spin chain is applicable for low-energy excitation.

The two-spinon confinement plays a key role in the quantized excitation spectra. On the other hand, the excitation continuum can be generated by other quasiparticles. A multi-magnon continuum in the $S = 1$ AF Heisenberg chain where a single magnon carries $\Delta S = 1$ is a typical candidate. In the $S = 1$ AF Heisenberg chain, the ground state is the celebrated Haldane-gap state [8–10]. It has been shown that, for low-energy excitation, the single-magnon isolated mode appears at $q \approx \pi$, while the lower edge of the two-magnon continuum is expected to be $q \approx 0$ [11–16]. At $q \approx \pi$, the lower edge of the three-magnon continuum appears above the single-magnon mode [11–16]. Despite these studies, however, low-energy excitations in the Q1D $S = 1$ AF spin system below T_N are still poorly understood. In this Rapid Communication, we focus on the quantized spectra in the Q1D $S = 1$ AF spin system with single-ion anisotropy and bond alternation.

The Hamiltonian for a Q1D $S = 1$ AF spin system with single-ion anisotropy and bond alternation is written as

$$\mathcal{H} = J \sum_{ij} [1 + \alpha(-1)^i] \boldsymbol{S}_{i,j} \cdot \boldsymbol{S}_{i+1,j}$$
$$+ D \sum_{ij} S_{i,j}^{z\ 2} + J' \sum_{i\langle j,j'\rangle} \boldsymbol{S}_{i,j} \cdot \boldsymbol{S}_{i,j'}, \quad (1)$$

where i is the site index in the chain direction and j specifies the chain. $J\ (>0)$ is the antiferromagnetic intrachain interaction and $J'\ (>0)$ is the interchain interaction. α denotes the bond alternation in the spin-chain direction and D represents the single-ion anisotropy. The summation $\langle j, j'\rangle$ runs over all nearest-neighbor interchain pairs. The bipartite system is assumed.

When the mean-field treatment for the weak interchain interaction is applied, the staggered fields are induced in the intrachain Hamiltonian. The effective Hamiltonian reads

$$\mathcal{H}_{\text{MF}} = J \sum_{i} [1 + \alpha(-1)^i] \boldsymbol{S}_i \cdot \boldsymbol{S}_{i+1}$$
$$+ D \sum_{i} S_i^{z2} + h_s \sum_{i} (-1)^i S_i^z, \quad (2)$$

where h_s is the mean field derived from the magnetic moments of the nearest-neighbor chains and is determined by solving a self-consistent equation. In the following calculations, we set a small value of h_s, because it is not important to obtain h_s self-consistently from a given J'.

We apply the infinite time-evolving block decimation algorithm [17,18] to calculate the dynamical spin structure factor (DSF) for the Hamiltonian (2). The DFS is defined as $S^{\mu\mu}(q,\omega) = \pi^{-1} \text{Im} \int \int i A^{\mu\mu}(x,t) e^{-iqx-i(\omega-e_g)t} dx dt$, where $A^{\mu\mu}(x,t) = \langle S_x^\mu(t) S_0^\mu(0) \rangle$ is the dynamical spin-spin correlation function and e_g is the ground-state energy. Note that $S_x^\mu(t) = e^{i\mathcal{H}_{MF}t} S_x^\mu e^{-i\mathcal{H}_{MF}t}$. The details of the numerical techniques have been discussed in Ref. [19]. We obtain the DSFs from the Fourier transformation of $A^{\mu\mu}(x,t)$ for a finite window size N in real space. To reduce numerical noise, we combine the Gaussian filtering method [20] with the Fourier transformation. In the following calculations, we set $\chi_{max} = 120$, where χ corresponds to the maximum value of the bond dimension for tensors composing the wave function, and $N = 200$ for the window size. We calculate the DSFs for $S = 1/2$ and $S = 1$ Heisenberg chains as a benchmark test, which are shown in Ref. [5].

In Fig. 1, we show the DSFs of the Hamiltonian (2) for $(\alpha, D/J) = (0, -5)$. When $(\alpha, D/J) = (0, -5)$ and $h_s = 0$, the ground state is the Néel state. Since the critical point between the Haldane and Néel phases exists at $D_c/J = -0.36 \pm 0.01$ [21] for $\alpha = 0$ and $h_s = 0$, $(\alpha, D/J) = (0, -5)$ is considered to be located deep in the Néel phase. For $(\alpha, D/J) = (0, -5)$, an isolated mode appears in $0 \leqslant q_x \leqslant \pi$ in the low-lying excitation [Figs. 1(a) and 1(b)]. The excitation continuum appears above the isolated mode. These excitation continua are quantized by the finite value of h_s, as shown in Figs. 1(c) and 1(d). In Figs. 1(e) and 1(f), the NZAF and each excitation energy of the quantized excitation spectra at $q_x = \pi$ and $\pi/2$ are compared. We find that the excitation energies of the quantized spectra in both $S^{xx}(q_x,\omega)$ [$= S^{yy}(q_x,\omega)$] and $S^{zz}(q_x,\omega)$ are quantitatively explained by NZAF. Note that the lowest quantized state is *not* the low-lying isolated mode.

Since each spin prefers the $S^z = \pm 1$ state for the negatively large D/J, the system is mapped to the AF Ising chain at the Ising limit, $D/J \to -\infty$, due to the positive J. For the bipartite system, the AF Ising chain is equivalent to the FM Ising chain via spin rotations on one of the two sublattices. The mapped Hamiltonian is expressed as $\mathcal{H}_{FM} = \mathcal{H}_0 + \mathcal{H}_1$, where $\mathcal{H}_0 = D \sum_i S_i^{z2} - J \sum_i S_i^z S_{i+1}^z - h_s \sum_i S_i^z$ and $\mathcal{H}_1 = J \sum_i (S_i^+ S_{i+1}^+ + S_i^- S_{i+1}^-)$. The condition $|D|/J \gg 1$ allows $\mathcal{H}_1$ to be treated as the perturbation. If h_s is positively infinitesimal, the ground state of $\mathcal{H}_0$ is the fully polarized state expressed by $\psi_{GS}^+ = |\cdots +++++++\cdots\rangle$, where $+$, 0, and $-$ in the ket denote $S^z = 1, 0$, and -1, respectively. When $\mathcal{H}_1$ is included, the total S_z is not a good index, but the Hilbert space is still classified by the parity of total S_z.

First, we consider the low-energy excitation in $S^{xx}(q_x,\omega)$. The low-energy excitation in $S^{xx}(q_x,\omega)$ is described by the dynamics of the state ψ_1^+ whose initial state is prepared by $\psi_1^+ = S_i^x |\psi_{GS}^+\rangle$. Since $S_i^x \propto (S_i^+ + S_i^-)$, this initial state is interpreted as one magnon state, $\psi_1^+ \propto |\cdots +++0+++\cdots\rangle$. The parity of ψ_1^+ is different from that of the ground state. Since the energy cost to create ψ_1^+ is approximately
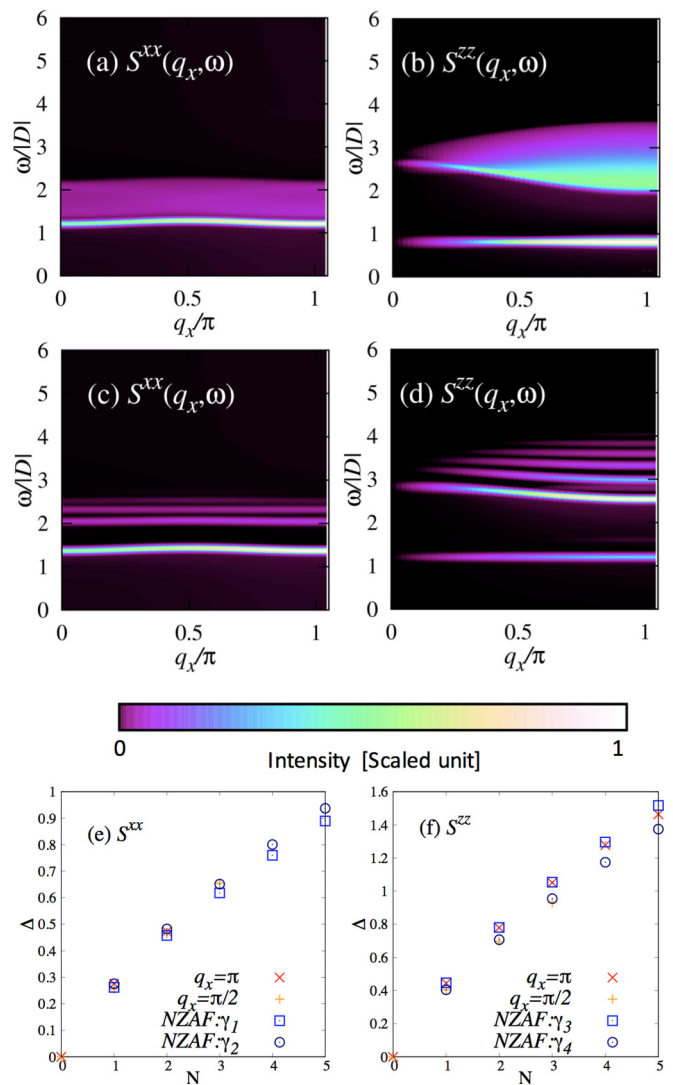

FIG. 1. $S^{xx}(q_x,\omega)$ and $S^{zz}(q_x,\omega)$ for $(\alpha, D/J) = (0, -5)$ at (a), (b) $h_s = 0$ and at (c), (d) $h_s/|D| = 0.1$. The excitation energies Δ of the quantized excitation spectra of (e) $S^{xx}(q_x,\omega)$ and (f) $S^{zz}(q_x,\omega)$ at $q_x = \pi$ and $\pi/2$. The horizontal axis corresponds to the excitation level of the quantized spectra. Note that the isolated mode that already emerged at $h_s = 0$ is excluded for counting the excitation levels. Δ is measured from the lowest quantized energy. The NZAF results are scaled using a constant factor γ_i to fit the excitation energy $\Delta(N=1)$ for the first excited state in the quantized excitation spectra, $\Delta = \gamma_i z_i$, where z_i indicates each negative zero of the Airy function. The constants used for the fitting are $\gamma_1 \approx 0.270$, $\gamma_2 \approx 0.285$, $\gamma_3 \approx 0.191$, and $\gamma_4 \approx 0.173$.

$\omega = |D| + 2J$, the isolated mode by ψ_1^+ appears at $\omega = |D| + 2J$, in the absence of $\mathcal{H}_1$. When $\mathcal{H}_1$ acts on the site with $S^z = 0$, the further excited state appears above ψ_1^+: $S^z = 0$ moves to the nearest-neighbor site, accompanying the site with $S^z = -1$, $|\cdots +++-0++\cdots\rangle$. This means that the domain composed of the $S^z = -1$ sites develops by the action of $\mathcal{H}_1$ on the site with $S^z = 0$ repeatedly. Therefore, the excitation continuum with the band center at $\omega \approx |D| + 4J$ appears above the excitation mode by the ψ_1^+ state. In the mapped Hamiltonian, h_s works as the confinement potential

for the domain with $S^z = -1$ sites, and thus the excitation continuum is quantized by h_s.

Next, the low-energy excitation in $S^{zz}(q_x, \omega)$ is considered. Since the initial state in the longitudinal component is given by multiplying the ground state at the site i by S_i^z, the parity of total S_i^z for the initial state is conserved. The $\mathcal{H}_1$ operation on a nearest-neighbor pair of the initial state creates the two-magnon state, namely, $\psi_2^+ = |\cdots + + + 00 + + + \cdots\rangle$. The energy cost for creating ψ_2^+ is $\omega \approx 2|D| + 3J$. For example, when $\mathcal{H}_1$ acts on ψ_2^+ twice at the sites with $S^z = 0$, each magnon moves in the opposite direction, $|\cdots + + 0 - - 0 + + \cdots\rangle$. Thus, the domain with $S^z = -1$ sites develops through the action of $\mathcal{H}_1$ repeatedly on the site with $S^z = 0$. This means that the domain-wall excitation is also allowed for ψ_2^+ and the excitation continuum appears centered at $\omega \approx 2|D| + 4J$. In the same manner as the excitation continuum by ψ_1^+, the excitation continuum by ψ_2^+ is quantized by h_s.

The quantization of the excitation continua discussed above is explained by NZAF, because the mechanism, namely, the confinement of the domain walls, is similar to that discussed for the $S = 1/2$ FM Ising spin chain [4]. The above scenario is considered to be satisfied for $D/J = -5$, which implies that the system is near the Ising limit. From the analogy to the domain-wall excitation in the $S = 1/2$ FM Ising spin chain [4], domain-wall excitation by $\psi_0^+ = |\cdots + + + - - + + + \cdots\rangle$ is expected to appear in the low-energy excitation. However, a higher-order process is required to create such a state and the intensity is much suppressed in the present case.

In Fig. 2, the DSFs for $(\alpha, D/J) = (0, -0.2)$ are shown, where the ground state is in the Haldane phase when $h_s = 0$. For $h_s = 0$, the single-magnon isolated mode appears in the low-lying excitation at $q_x \approx \pi$ and the multimagnon continuum appears above the isolated mode, which is schematically the same behavior as that of the isotropic case $D = 0$ [11–16]. Even for $(\alpha, D/J) = (0, -0.2)$, the quantization of the excitation continuum emerges for $h_s > 0$. However, the quantization is not clear in comparison with that for $D/J = -5$. In Figs. 2(e) and 2(f), the NZAF and excitation energies of the quantized spectra at $q_x = \pi$ and $\pi/2$, respectively, are compared. For $(\alpha, D/J) = (0, -0.2)$, the excitation energies of the quantized spectra in $S^{xx}(q_x, \omega)$ and $S^{zz}(q_x, \omega)$ deviate from NZAF. Note that the energy of the third quantized state ($N = 3$) in $S^{zz}(q_x = \pi, \omega)$ accidentally agrees with that of NZAF. Therefore, the origin of quantization in the excitation spectra is considered to be different from that in the Ising limit.

For $(\alpha, D/J) = (0, -0.2)$ and $h_s = 0$, the system is in proximity to the phase boundary between the Haldane and Néel phases. At the critical point, the energy gap closes and the system is described by the Tomonaga-Luttinger liquid in the low-energy limit [22], which is equivalent to the theory of free boson fields. When the system departs from the critical point, the low-energy effective model is expressed by adding the family of $C_b \exp[ib\phi]$ terms [23] to the Lagrangian of free-boson field theory, where ϕ is the bosonic field and b and C_b are constants. Each $C_b \exp[ib\phi]$ is classified as relevant or irrelevant, and the most relevant interaction opens the energy gap. This means that the sine-Gordon field theory qualitatively describes the low-energy part of the system in proximity
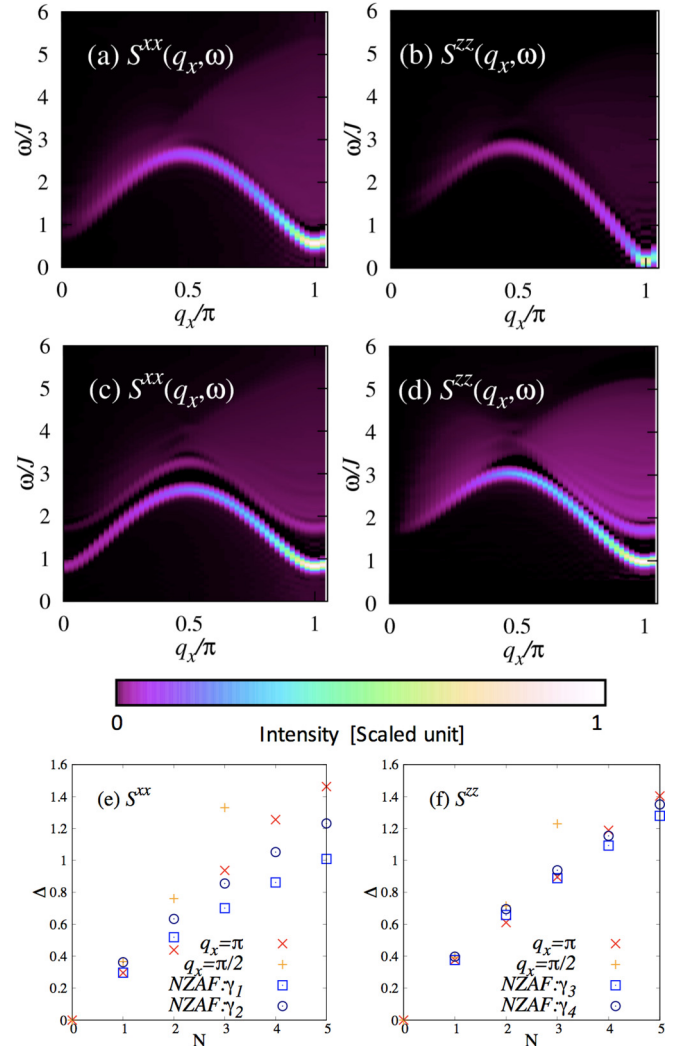

FIG. 2. $S^{xx}(q_x, \omega)$ and $S^{zz}(q_x, \omega)$ for $(\alpha, D/J) = (0, -0.2)$ at (a), (b) $h_s = 0$ and (c), (d) $h_s/J = 0.1$. The excitation energies of the quantized excitation spectra of (e) $S^{xx}(q_x, \omega)$ and (f) $S^{zz}(q_x, \omega)$ at $q_x = \pi$ and $\pi/2$. The constants used for the fitting are $\gamma_1 \approx 0.127$, $\gamma_2 \approx 0.155$, $\gamma_3 \approx 0.163$, and $\gamma_4 \approx 0.170$.

to the phase boundary. In the excitation spectrum of the sine-Gordon field theory, several isolated modes originating from the soliton/antisoliton and breather modes are present in addition to the excitation continuum [22]. When the system approaches the critical point, the excitation continuum shifts to the lower-energy region and the isolated modes become unstable by touching the lower edge of the excitation continuum. However, when the system deviates from the critical point, these isolated modes are placed below the lower edge of the excitation continuum and thus we observe the quantized excitation spectra. This scenario for the quantized excitation spectra is considered valid in the vicinity of the following two critical lines: One is dividing the Néel and Haldane phases, and the other is dividing the Néel and singlet-dimer phases, as shown in Fig. 3(a).

In Fig. 3(a), the region where the quantized excitation spectra appear for $h_s > 0$ is schematically represented by the shaded area. Figures 3(b)–3(e) are the results of
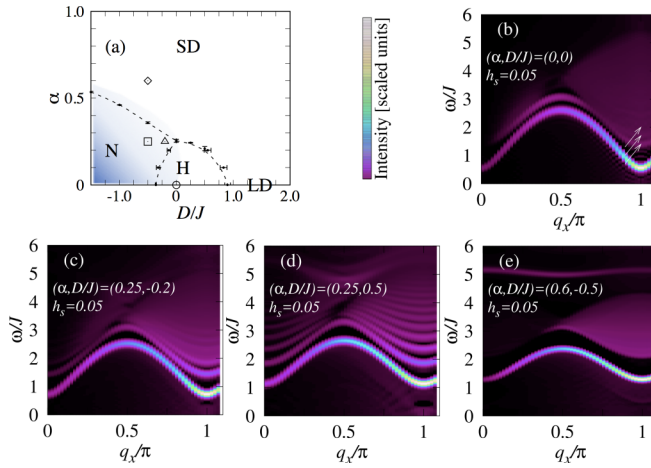
FIG. 3. (a) Schematic region where the quantized excitation spectra are observed. In the shaded area, the excitation continuum shows the quantization for $h_s > 0$. Black dots are critical points at $h_s = 0$, presented in Ref. [21]. "H," "N," "SD," and "LD" correspond to the Haldane phase, Néel phase, singlet-dimer phase, and large-D phase, respectively. (b)–(e) $S^{xx}(q_x, \omega)$ at $(\alpha, D/J) = (0, 0)$, $(0.25, -0.2)$, $(0.25, -0.5)$, and $(0.6, -0.5)$ for $h_s = 0.05$. Open circle, triangle, square, and diamond in (a) correspond to the parameter used in (b)–(e) for $h_s = 0$, respectively. Note that the DSFs are shown in the extended zone representation except for (b). White arrows in (b) indicate the peak positions of the intensity.

$S^{xx}(q_x, \omega)$ at $(\alpha, D/J) = (0, 0)$, $(0.25, -0.2)$, $(0.25, -0.5)$, and $(0.6, -0.5)$. Since the large intensity appears at $q_x = \pi$ and $\omega = 0$ in $S^{zz}(q_x, \omega)$ deep in the Néel phase [5], the relative intensity of the quantized excitation spectra in $S^{zz}(q_x, \omega)$ is very weak.

For $(\alpha, D/J) = (0, 0)$, $(0.25, -0.2)$, and $(0.25, -0.5)$, the system with the first parameter is located in the Haldane phase and the latter two are located in the Néel phase for $h_s = 0$. In such a case, the excitation continuum in the DSF is quantized for $h_s > 0$, as shown in Figs. 3(b)–3(d). The quantization of the spectra is smeared when the system approaches the phase boundary in the singlet-dimer phase. The quantized excitation spectra disappear in the singlet-dimer phase, as shown in Fig. 3(e). This is explained by considering the low-energy excitation for $D = 0$ and $\alpha \approx 1$. For $D = 0$ and $\alpha \approx 1$, the ground state is the direct product state of the singlet dimers. The low-energy excitation that has a potential to compose the excitation continuum is given by replacing two singlets with two triplets from the ground state. As α decreases from $\alpha = 1$,

the two-triplet excitation composes the excitation continuum around $q_x = \pi$ [24]. However, the staggered field does not work as the confinement potential and rather localizes the triplet dimers with $S^z = 0$. Note that the energy of the triplet dimer with $S^z = \pm 1$ remains unchanged by the staggered field, which means that the confinement potential is absent.

At $D \to \infty$, the ground state is expressed by the direct product of $S^z = 0$ at each site, namely, $\psi_0 = |\cdots 00000000 \cdots\rangle$. The lowest-energy excitation from ψ_0 is given by the single-spin flipping, $\psi_1^+ = |\cdots 000 + 000 \cdots\rangle$ or $\psi_1^- = |\cdots 000 - 000 \cdots\rangle$. The site carrying $S^z = \pm 1$ propagates by the hopping term $S_i^+ S_{i+1}^- + S_i^- S_{i+1}^+$, and $\psi_1^\pm$ composes the isolated mode. The candidate for the low-energy excitation that composes the excitation continuum is obtained by creating two $S^z = 1$ ($S^z = -1$) states at the neighboring sites, $\psi_2^+ = |\cdots 000 + +000 \cdots\rangle$ or $\psi_2^- = |\cdots 000 - -000 \cdots\rangle$. In $\psi_2^\pm$, each site with $S^z = 1$ (or $S^z = -1$) almost freely travels in the chain, and thus they compose the excitation continuum. However, since all sites sandwiched by the two sites with $S^z = 1$ (or $S^z = -1$) are filled by $S^z = 0$ due to the energy cost, the staggered field does not work as the confinement potential for the two sites with $S^z = 0$. Thus, the quantized excitation spectra are suppressed in the singlet-dimer phase [5].

So far, many $S = 1$ chain materials have been synthesized. Most of them are considered to have the positive single-ion anisotropy, but negative single-ion anisotropy has been also reported for several materials. For example, Y_2BaNiO_5 [25] and $SrNi_2V_2O_8$ [26] have been evaluated as $D/J \approx -0.033$ and ≈ -0.057, respectively. There are likely many compounds whose proper models have been unsettled precisely due to the large deviation from the ideal Haldane-gap system. In such compounds, there is a chance to find the quantized excitation spectra. Further experiments are desirable.

[1] B. Grenier, S. Petit, V. Simonet, E. Canévet, L.-P. Regnault, S. Raymond, B. Canals, C. Berthier, and P. Lejay, Phys. Rev. Lett. **114**, 017201 (2015).

[2] Q. Faure, S. Takayoshi, S. Petit, V. Simonet, S. Raymond, L.-P. Regnault, M. Boehm, J. S. White, M. Månsson, C. Rüegg, P. Lejay, B. Canals, T. Lorenz, S. C. Furuya, T. Giamarchi, and B. Grenier, Nat. Phys. **14**, 716 (2018).

[3] S. Kimura, H. Yashiro, K. Okunishi, M. Hagiwara, Z. He, K. Kindo, T. Taniyama, and M. Itoh, Phys. Rev. Lett. **99**, 087602 (2007).

[4] B. M. McCoy and T.-T. Wu, Phys. Rev. D **18**, 1259 (1978).

[5] See Supplemental Material at http://link.aps.org/supplemental/10.1103/PhysRevB.98.180406 for the benchmark test of the infinite time-evolving block decimation algorithm. In addition, we have summarized the discussion in Ref. 4 briefly, and have shown the longitudinal and transverse DSFs for five values of $(\alpha, D/J)$ that correspond to the four phases in Fig. 3.

[6] R. Coldea, D. A. Tennant, E. M. Wheeler, E. Waerzynska, D. Prabhakaran, M. Telling, K. Habicht, P. Seibidl, and K. Kiefer, Science **327**, 177 (2010).

[7] H. Shiba, Prog. Theor. Phys. **64**, 466 (1980).

[8] F. D. M. Haldane, Phys. Lett. A **93**, 464 (1983).

[9] F. D. M. Haldane, Phys. Rev. Lett. **50**, 1153 (1983).

[10] I. Affleck, T. Kennedy, E. H. Lieb, and H. Tasaki, Phys. Rev. Lett. **59**, 799 (1987); Commun. Math. Phys. **115**, 477 (1988).

[11] M. Takahashi, Phys. Rev. Lett. **62**, 2313 (1989); Phys. Rev. B **48**, 311 (1993); **50**, 3045 (1994).

[12] S. R. White, Phys. Rev. Lett. **69**, 2863 (1992); S. R. White and D. A. Huse, Phys. Rev. B **48**, 3844 (1993).

[13] I. Affleck and R. A. Weston, Phys. Rev. B **45**, 4667 (1992).

[14] S. Yamamoto and S. Miyashita, Phys. Lett. A **235**, 545 (1997).

[15] M. D. P. Horton and I. Affleck, Phys. Rev. B **60**, 11891 (1999).

[16] F. H. L. Essler, Phys. Rev. B **62**, 3264 (2000).

[17] G. Vidal, Phys. Rev. Lett. **98**, 070201 (2007).

[18] R. Orús and G. Vidal, Phys. Rev. B **78**, 155117 (2008).

[19] H. N. Phien, G. Vidal, and I. P. McCulloch, Phys. Rev. B **86**, 245107 (2012).

[20] S. R. White and A. E. Feiguin, Phys. Rev. Lett. **93**, 076401 (2004).

[21] T. Tonegawa, T. Nakano, and M. Kaburagi, J. Phys. Soc. Jpn. **65**, 3317 (1996).

[22] J. Tamaki and M. Oshikawa, Phys. Rev. B **85**, 134431 (2012), and references therein.

[23] S. Sachdev, *Quantum Phase Transitions* (Cambridge University Press, Cambridge, UK, 1999).

[24] T. Suzuki and S.-i. Suga, Phys. Rev. B **68**, 134429 (2003).

[25] G. Xu, J. F. DiTusa, T. Ito, K. Oka, H. Takagi, C. Broholm, and G. Aeppli, Phys. Rev. B **54**, R6827(R) (1996).

[26] A. K. Bera, B. Lake, A. T. M. N. Islam, B. Klemke, E. Faulhaber, and J. M. Law, Phys. Rev. B **87**, 224423 (2013).